Eur Phys J A (2004) **19**, s01, 249–256
Digital Object Identifier (DOI) 10.1140/epjad/s2004-03-041-9

EPJ A direct
electronic only

Selected recent HERMES results

Klaus Rith, on behalf of the HERMES collaboration

Physikalisches Institut, Universität Erlangen-Nürnberg, D-91058 Erlangen

Received: 19 Aug 2003 / Accepted: 14 Nov 2003 /
Published Online: 6 Feb 2004 –

Abstract. The first phase of HERMES data taking covers the years 1995 to 2000. Data were taken with longitudinally polarised ^{3}He (1995), hydrogen (1996-1997) and deuterium (1998-2000) targets, but also with several other unpolarised targets (H_2, D_2, ^{3}He, ^{4}He, N_2, Ne and Kr). Some selected results from this data taking period are discussed: the spin-dependent structure function g_1 from deuterium, which has been measured with high accuracy down to $x = 0.0021$; quark and antiquark helicity distributions from semi-inclusive deep-inelastic scattering on hydrogen and deuterium, which indicate that the antiquark distributions are consistent with zero and with each other and do not favour a substantial negative polarisation of the strange quark sea; and the first measurement of nuclear attenuation of identified fast charged and neutral pions, charged kaons, protons and antiprotons produced from nitrogen and krypton targets.

PACS. 13.60.-r – 13.87.Fh – 13.88.+e – 14.20.Dh – 14.40.-n – 14.65.-q

1 Introduction

HERMES is one of the four experiments at the HERA electron proton collider at DESY. It uses the high current longitudinally polarised electron or positron beams of HERA with a beam energy E of about 27.6 GeV together with polarised and unpolarised gas targets internal to the storage ring. Scattered electrons and particles produced in the deep-inelastic electron-nucleon interactions are detected and identified by an open-geometry forward spectrometer with large momentum and solid angle acceptance [1]. HERMES is based on two special techniques: longitudinal electron polarisation in a high energy storage ring [2], which is achieved by a system of spin rotator magnets [3], and a storage cell target [4] where the nuclear-polarised atoms from a high intensity polarised source [5, 6] are present as pure atomic species without dilution from unpolarised target material.

The primary scientific goal of HERMES was and still is the detailed investigation of the spin structure of the nucleon. But the physics reach of the experiment extends well beyond this specific aspect of hadronic physics and the experiment explores many details of hadron structure, hadron production and hadronic interactions with electromagnetic probes at cen-tre-of-mass energies $\sqrt{s}$ of around 7 GeV.

The first phase of HERMES data taking covers the years 1995 to 2000. Data were taken with longitudinally polarised ^{3}He (1995), hydrogen (1996-1997) and deuterium (1998-2000) targets, but also with several other unpolarised targets (H_2, D_2, ^{3}He, ^{4}He, N_2, Ne and Kr). These data yielded a lot of high precision results on inclusive and semi-inclusive polarised deep-inelastic scattering and have confirmed and extended our understanding of the contribution of quark spins to the spin of the nucleon. The results include: the measurement of the spin-dependent structure function g_1 for ^3He, H and D, the determination of the generalised Drell-Hearn-Gerasimov integral for proton, neutron and deuteron, the flavour decomposition of the quark helicity distributions from semi-inclusive polarised deep-inelastic scattering, a first indication of a positively polarised gluon distribution from a double-spin asymmetry in the production of pairs of hadrons with high transverse momenta, the observation of a double-spin asymmetry in the cross section for exclusive electro-production of vector mesons, an experimental indication for effects of transversity in the nucleon, azimuthal single-spin asymmetries in hard exclusive electroproduction of real photons and pions which can be related to generalised parton distributions, the investigation of longitudinal spin-transfer in electro-production of Λ hyperons in the current fragmentation region and the observation of a positive transverse polarisation of Λ particles produced in quasi-real photo-production. A comprehensive review of these results on spin-asymmetries in deep-inelastic electron-nucleon scattering can be found in [7]. Additional results include: the determination of a flavour asymmetry in the light quark sea from charged pion production from unpolarised hydrogen and deuterium targets [8], multiplicity distributions in pion electro-production [9], cross sections and decay angular distributions for hard exclusive electro-production of vector mesons [10,11], the first observation of a coherence length effect on exclusive coherent and incoherent electro-production of ρ^0 mesons

from nuclear targets and their Q^2 dependence [12,13], and the measurement of the attenuation of fast hadrons produced from nuclear targets [14,15]. Many more results from ongoing analyses- based on data collected in this first phase of data taking will be published in the near future. In this paper only a few aspects are discussed: the spin-dependent structure function g_1 from deuterium, quark and antiquark helicity distributions from semi-inclusive deep-inelastic scattering on D and H, and the attenuation of fast hadrons produced from nuclear targets.

The second phase of HERMES data taking will cover the years until the end of 2006. The physics program, which is summarised in the contribution by W.D. Nowak to this conference [16], will concentrate on measurements with a transversely polarised hydrogen target for a first determination of the so-called *transversity* distribution and measurements with high density unpolarised hydrogen targets in conjunction with a new recoil detector around the storage cell target to study in detail hard exclusive processes.

2 The spin-dependent deuteron structure function $g_1^d(x, Q^2)$

In the years 1998 to 2000 data were taken at HERMES with the longitudinally polarised deuterium target. Altogether about 9 million DIS events were collected, corresponding to an integrated luminosity of about 80 pb^{-1}. The average beam polarisation was $\langle|P^{\rm B}|\rangle = 0.53$ and the average target polarisation $\langle|P^{\rm T}|\rangle = 0.845$. The kinematic range of the data is $0.0021 < x < 0.85$, $0.1 < y < 0.91$, $Q^2 > 0.1$ GeV^2 and $W^2 > 3.24$ GeV^2. Here $x = Q^2/2M\nu$ is the Bjorken variable, $-Q^2$ is the squared four-momentum transfer, M is the nucleon mass, ν is the energy of the virtual photon, $y = \nu/E$, and W is the invariant mass of the photon-nucleon system.

The preliminary HERMES result for the structure function ratio $g_1^{\rm d}/F_1^{\rm d}$ for the data from the year 2000 is shown in Fig. 1 together with the corresponding data from SMC [17], E143 [18] and E155 [19]. Here

$$g_1^d(x,Q^2) = \frac{1}{2}[g_1^p + g_1^n](x,Q^2) = \frac{1}{4}\sum_q e_q^2\ \Delta q(x,Q^2) \quad (1)$$
$$= \frac{5}{36}[\Delta u + \Delta\bar{u} + \Delta d + \Delta\bar{d} + \Delta s + \Delta\bar{s}](x,Q^2)$$
$$-\frac{1}{12}[\Delta s + \Delta\bar{s}](x,Q^2)$$

is the spin-dependent structure function and F_1^d the corresponding spin-independent structure function. $\Delta q(x,Q^2)$ is the quark helicity distribution for flavour q and e_q is the quark charge in units of the elementary charge. For each data point in x the mean Q^2 is different for each experiment as can be seen from the lower panel of the figure. The seven data points from SMC at even lower values of x down to $x \cong 10^{-4}$ are not shown here. No corrections for smearing effects, which will increase somewhat the error bars and influence the central values mainly at very low x, have been applied yet to these preliminary HERMES data. They have substantially smaller error bars and much smaller point to point fluctuations than those from the other experiments, and determine the x dependence of this ratio now very well. This is especially evident in the range of very small x, but also at higher x where the central values of various previous data sets scattered substantially. At x below about 0.03 the asymmetry is compatible with zero, with a slight tendency to negative values. One can conclude from this behaviour that at these small x values Δd(x) and Δu(x) have about the same magnitude, but opposite sign. If the asymmetry really gets negative then one can speculate that either the magnitude of the down-quark helicity distribution must get bigger than the up-quark helicity distribution or that the net sea-quark helicity distribution must be negative. At large x the rise of the asymmetry with x is much less steep than for the proton data [17,18,20,21,22], the limit at $x \to 1$ possibly being substantially smaller than unity.

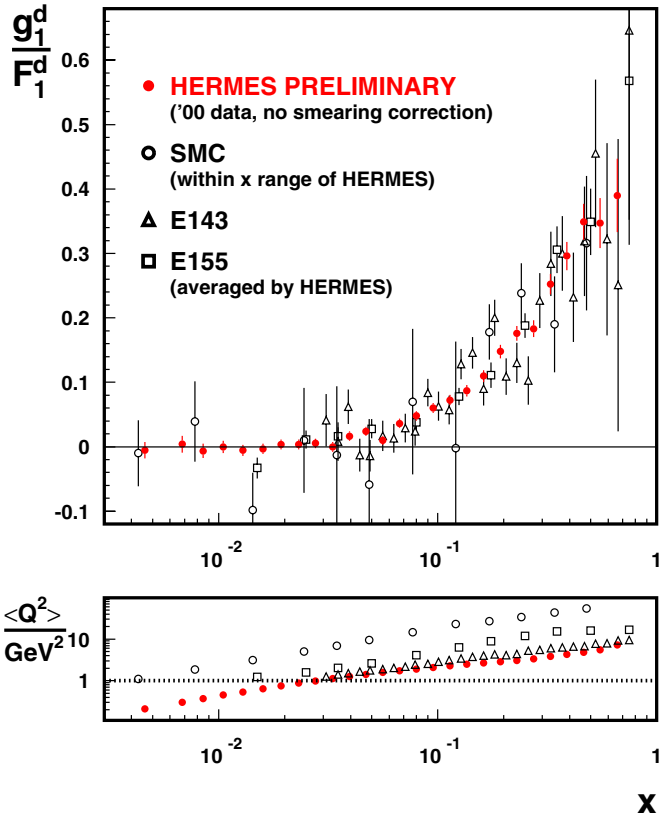

Fig. 1. Preliminary HERMES results for the structure function asymmetry $g_1^{\rm d}/F_1^{\rm d}$ as a function of x together with the corresponding data from E143, E155 and SMC in the x range covered by the HERMES data

The preliminary HERMES result from the 2000 data for $g_1^{\rm d}(x)$ at the measured values of Q^2 is shown as a function of x together with the corresponding data from SMC in Fig. 2. It is evident that with these new data also the x dependence of $g_1^{\rm d}$ is very well determined in the range $x > 2\cdot10^{-3}$. Below x values of about $3\cdot10^{-2}$ it is compatible with zero with a slight tendency to negative values.

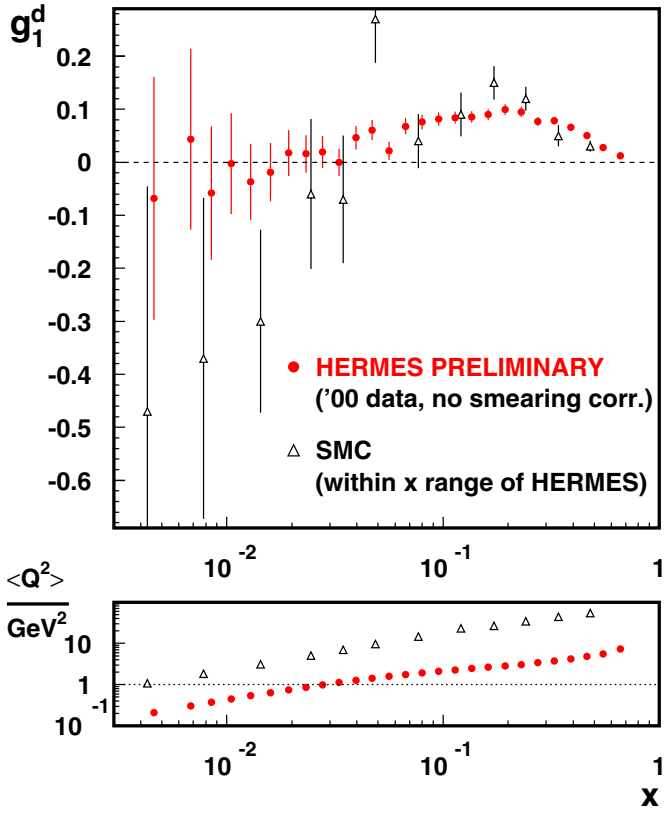

Fig. 2. Preliminary HERMES results for the structure function g_1^{d} together with the SMC results at the measured values of Q^2 as a function of x in the x range covered by the HERMES data

3 Quark helicity distributions from semi-inclusive DIS

3.1 Semi-inclusive asymmetries

The up-quark helicity distribution, $\Delta\mathrm{u}(x)$, is rather well constrained by the inclusive polarised proton and deuteron data as well in shape as in magnitude, while NLO-QCD fits, like e.g. [23,24,25,26] give a much larger possible range for $\Delta\mathrm{d}(x)$. The sea-quark helicity distributions and especially $\Delta\mathrm{s}(x)$ are essentially undetermined from such fits and very different solutions are possible for the gluon helicity distribution $\Delta g(x)$. A detailed understanding of the spin structure of the nucleon requires, therefore, a direct determination of the x-dependence and of the moments of the helicity distributions of quarks and anti-quarks of the various flavours, and of the gluon. This can in principle be achieved in semi-inclusive spin-dependent deep-inelastic scattering when in addition to the scattered lepton also a leading hadron is detected. Since the charge and the identity of high energy forward hadrons are correlated to the flavour of the struck quark, this type of reaction can be used to study the flavour dependence of the quark helicity distribution. Precise double-spin asymmetries in the cross sections for leptoproduction of various types of hadrons allow a separation of the individual contributions of each quark flavour to the nucleon spin.

In leading order (LO) QCD, the semi-inclusive cross section for the production of a particular hadron h takes the factorised form

$$\sigma^h(x,z) \propto \sum_q e_q^2\, q(x)\, D_q^h(z)\ , \tag{2}$$

where the fragmentation function $D_q^h(z)$, which parameterises all our ignorance of the non-perturbative fragmentation process, is the probability density that a struck quark of flavour q fragments into a hadron h with energy E_h, or fractional virtual photon energy $z = E_h/\nu$, respectively. For simplicity the weak logarithmic dependence on Q^2 is suppressed here. The double-spin asymmetry A_1^h in the above cross section is then given by

$$A_1^h(x) = \frac{\sum_q e_q^2 \Delta q(x)\, D_q^h(z,)}{\sum_{q'} e_{q'}^2 q'(x)\, D_{q'}^h(z)} \cdot \frac{1+R(x)}{(1+\gamma^2)}, \tag{3}$$

where the factor involving $\gamma^2 = Q^2/\nu^2$ and R, the ratio of longitudinal to transverse virtual photon cross sections, accounts for the longitudinal component that is included in experimentally determined parameterisations of $q(x)$ but not in $\Delta q(x)$. It is assumed that the spin-dependent and spin-independent fragmentation functions are the same at least for pseudo-scalar mesons like pions and kaons.

3.2 Quark polarisations and purities

Integrating (2) over the range $0.2 \le z \le 0.8$, where one can assume that the hadrons originated from the struck quark and not from the target remnant and where also the contribution from exclusive processes is small, (3) becomes

$$A_1^h(x_i) = \sum_q P_q^h(x_i) \cdot \frac{\Delta q(x_i)}{q(x_i)} \cdot \frac{1+R(x)}{(1+\gamma^2)}\ , \tag{4}$$

where $\Delta q(x_i)/q(x_i)$ are the quark polarisations and $P_q^h(x_i)$ are the spin-independent purities:

$$P_q^h(x_i) \equiv \frac{e_q^2 q(x_i, Q_i^2)\, \mathcal{D}_q^h(x_i, z_i, Q_i^2)}{\sum_{q'} e_{q'}^2 q'(x_i, Q_i^2)\, \mathcal{D}_{q'}^h(x_i, z_i, Q_i^2)}\ . \tag{5}$$

Here $\mathcal{D}_q^h(x_i, z_i, Q_i^2)$ are *effective* fragmentation functions in a bin i with mean values of the kinematical quantities x_i, z_i, and Q_i^2 derived by averaging over all events in the bin, which take into account also the acceptance function of the spectrometer. Note that these purities only depend on one single parameter x_i in this definition, as the mean values Q_i^2 and z_i are fixed within one x-bin i.

The purities may be interpreted as the probability that, in a given bin of x, the photon struck a quark of type q in the nucleon when a hadron of type h is detected in the experiment. Obviously, the purities for each hadron species add up to one in each bin.

The purities provide a simple way to separate the quark polarisations from other quantities, which are related to unpolarised quark distributions and fragmentation functions. Their input parameters are known with good precision from a large number of DIS experiments on unpolarised targets, augmented by data on fragmentation functions from e^+e^- annihilation experiments.

For the determination of the various quark polarisations one combines inclusive asymmetries and semi-inclusive asymmetries for positive and negative hadrons and for identified hadrons of different species from various targets and obtains a system of linear equations which can be written for each bin i in a matrix form as:

$$\mathbf{A}\,(x_i) = \mathbf{P}\,(x_i)\,\mathbf{Q}\,(x_i)\ . \qquad (6)$$

Here the vector $\mathbf{A}$ contains as elements the measured inclusive and semi-inclusive hadron asymmetries for the various targets, the vector $\mathbf{Q}$ contains the quark and antiquark polarisations for each flavour and $\mathbf{P}$ is the purity matrix with elements P_q^h. This system of asymmetries is typically over-determined, as the number of measured asymmetries is larger than the number of various quark polarisations to be extracted.

The polarisations for each bin x_i are then obtained by solving (6) for the vector $\mathbf{Q}$ by χ^2-minimisation, accounting for the correlations between x-bins and between the various asymmetries.

3.3 Quark and antiquark helicity distributions

The high statistics deuterium data allowed a precise determination of semi-inclusive double-spin asymmetries for identified positive and negative pions and kaons. Together with the semi-inclusive asymmetries for positive and negative hadrons from the proton target [27] and the inclusive proton and deuteron asymmetries eight different asymmetries could be used as input for the asymmetry vector $\mathbf{A}(x) = (A_{1p}, A_{1p}^{\pi+}, A_{1p}^{\pi-}, A_{1d}, A_{1d}^{\pi+}, A_{1d}^{\pi-}, A_{1d}^{K+}, A_{1d}^{K-})$. The large data sample allowed a five parameter fit using the following polarisation vector:

$$\mathbf{Q}(x) = \left(\frac{\Delta u}{u}, \frac{\Delta d}{d}, \frac{\Delta \bar{u}}{\bar{u}}, \frac{\Delta \bar{d}}{\bar{d}}, \frac{\Delta s}{s}, \frac{\Delta \bar{s}}{\bar{s}} \equiv 0 \pm \frac{1}{\sqrt{3}}\right). \qquad (7)$$

The quark and antiquark helicity distributions $\Delta q(x)$ are determined as the product of the extracted polarisations and the corresponding spin-independent parton distribution functions [29] at the mean $\langle Q^2 \rangle = 2.5\ GeV^2$ of the present work. The results [28] are shown in Fig. 3 together with two LO-QCD fits [25,26] to previously published inclusive data.

In these fits the first moments of the valence helicity distribution Δu_v and Δd_v have been constrained using the F and D decay constants experimentally determined from the weak decays of the members of the spin-$\frac{1}{2}$ baryon octet. Explicitly flavour symmetry among the three sea-quark helicity distributions has been assumed in order to reduce the number of free fit parameters. Together with the above constraint this leads to a small and slightly negative sea-quark helicity distribution. The helicity distributions $\Delta u(x)$ and $\Delta d(x)$ extracted from the HERMES data are consistent with previous (semi)-inclusive results and with the LO-QCD fits. $\Delta u(x)$ is positive and $\Delta d(x)$ is negative over the measured range of x. Over most of the x-range the ratio of the magnitude of the two distributions is around 0.4, which is consistent with the negative value of $g_1^n(x)$ but substantially larger than the ratio $\frac{1}{4}$ predicted for the moments in the naive quark parton model. The sea-quark helicity distributions $\Delta\bar{u}(x)$, $\Delta\bar{d}(x)$ and $\Delta s(x)$, extracted separately from these data for the first time, are consistent with zero and with each other. The statistical error bars are, however, still substantially larger than the magnitude of the distribution obtained from the NLO-QCD fits. Within errors there is no indication for a substantial negative polarisation of the strange sea that was deduced from the analysis of only inclusive data assuming SU(3) symmetry, but given the size of the errors it is difficult to conclude whether there really is a disagreement or not.

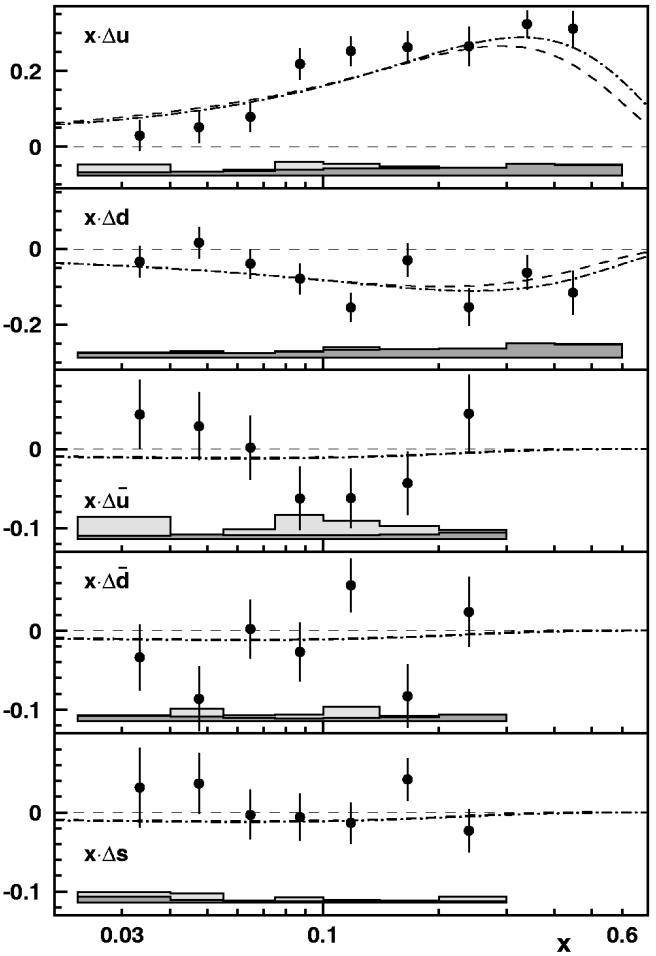

Fig. 3. Quark helicity distributions at $\langle Q^2 \rangle = 2.5\ GeV^2$ as a function of x compared to two LO QCD fits to previously published inclusive data shown as dashed [25] and dot-dashed [26] curves

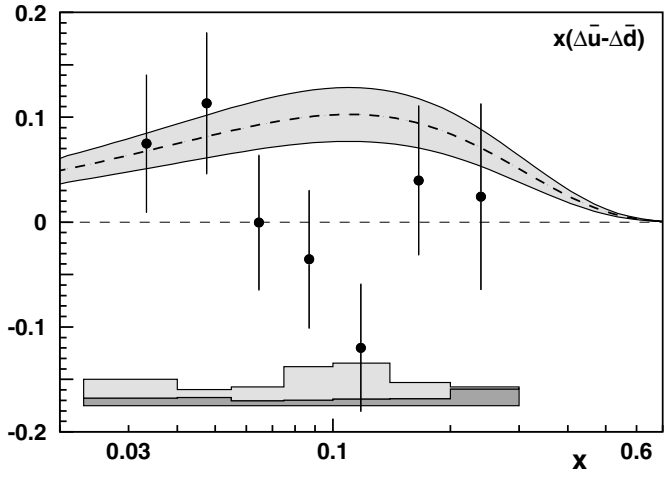

Fig. 4. The light quark sea flavour asymmetry $\Delta\bar{u} - \Delta\bar{d}$ in the helicity distributions, at $\langle Q^2 \rangle = 2.5\ GeV^2$, compared to a theoretical prediction [30] (*dashed curve with theoretical uncertainty band*)

Figure 4 shows the difference of the light quark sea helicity distribution $\Delta\bar{u}(x) - \Delta\bar{d}(x)$ together with a theoretical prediction of this quantity based on the chiral quark soliton model [30]. There is no evidence in the data for a large flavour asymmetry, and the data appear to be below the theoretical prediction. Given the substantial point to point fluctuations there is, however, no real discrepancy between this theoretical prediction and the experimental data.

4 Hadronisation in nuclei

In QCD hadrons are colourless objects and quarks with nonzero colour quantum number can therefore not exist as free particles. This phenomenon of confinement leads to the process of hadronisation in high energy reactions like deep-inelastic scattering: as well the struck quark as the target remnant have to fragment into hadrons. This fragmentation process is described by the fragmentation function $D_q^h(z)$, introduced above, which is a measure for the probability that a quark of flavour q produces a hadron of type h carrying a fraction z of the energy of the struck quark in the target rest frame.

Experimental information on the hadronisation process can be obtained by embedding the formation process in an atomic nucleus. The nuclear environment may thereby influence the hadronisation process for instance by multiple interactions of the quark with the surrounding medium and induced gluon radiation resulting in energy loss of the quark and thereby a reduction of the hadron yield at high z. If the hadron is formed inside the nucleus, the hadron can interact via the relevant hadronic interactions, causing a further reduction of the hadron yield. This reduction depends on the distance traversed by the quark before the hadron is formed which is proportional to the so called formation time and the quark energy ν. At high ν the hadron will be formed outside the nucleus and the reduction of yield will be small. By studying the properties of leading hadrons emerging from nuclei, information on the characteristic time-distance scales of hadronisation can be derived. The understanding of quark propagation in the nuclear medium is crucial for the interpretation of ultra-relativistic heavy ion collisions, as well as high energy proton-nucleus and lepton-nucleus interactions [31].

Theoretical descriptions of the hadronisation process in the nuclear medium include phenomenological string models, final state interactions of the hadrons with the surrounding medium or in-medium modifications of the quark fragmentation functions due to different origins like parton energy loss, higher twist contributions or gluon bremsstrahlung. For a collection of corresponding references see [14,15], some aspects of the different approaches have been discussed at this conference [32].

The HERMES experiment is ideally suited for such studies: the energy domain ranges from about 2 to 23 GeV and the corresponding length scales involved in the hadronisation process are of the same order as the nuclear size, the nuclear sizes of a few fm can be varied by using several atomic species ranging from hydrogen to krypton, and the gaseous targets are so dilute that very little secondary interactions of the produced hadrons with the target material occur. The dual-radiator RICH detector [33] allows to identify pions, kaons, protons and antiprotons over most of the kinematic range covered by the spectrometer and to study the nuclear effects separately for these different hadron species.

The experimental results for semi-inclusive deep-inelas-tic scattering on nuclei are usually presented in terms of the hadron multiplicity ratio R_M^h, which is defined as the number of hadrons of type h produced per deep-inelastic scattering event for a nuclear target of mass A to that from a deuterium target (D). This ratio depends on ν, Q^2, z and p_t^2, where p_t is the hadron momentum component transverse to the virtual photon direction.

The multiplicity ratio is defined as:

$$R_M^h(z,\nu,p_t^2,Q^2) = \frac{\left.\frac{N_h(z,\nu,p_t^2,Q^2)}{N_e(\nu,Q^2)}\right|_A}{\left.\frac{N_h(z,\nu,p_t^2,Q^2)}{N_e(\nu,Q^2)}\right|_D}, \qquad (8)$$

where N_h is the yield of semi-inclusive hadrons in a given (z,ν,p_t^2,Q^2)-bin, and N_e the yield of inclusive deep-inelastic scattering leptons in the same (ν,Q^2)-bin. In the following the ratio R_M^h is evaluated as a function of ν, z and p_t^2, while integrating over all other kinematic variables.

In this contribution results are presented on the hadron multiplicities on krypton ^{84}Kr and nitrogen ^{14}N relative to deuterium for beam energies of 12 and 27.6 GeV. These are the first measurements of the multiplicity ratio for identified charged and neutral pions, charged kaons, protons and antiprotons. Additionally the previously published [14] nitrogen data for charged hadrons and identified pions are reevaluated, now covering a wider kinematic range. The 27.6 GeV krypton data were obtained during dedicated runs in 1999, when high density krypton gas was injected into the storage cell and target areal densities up to 1.4×10^{16} nucleons per cm^2 were obtained. This made it

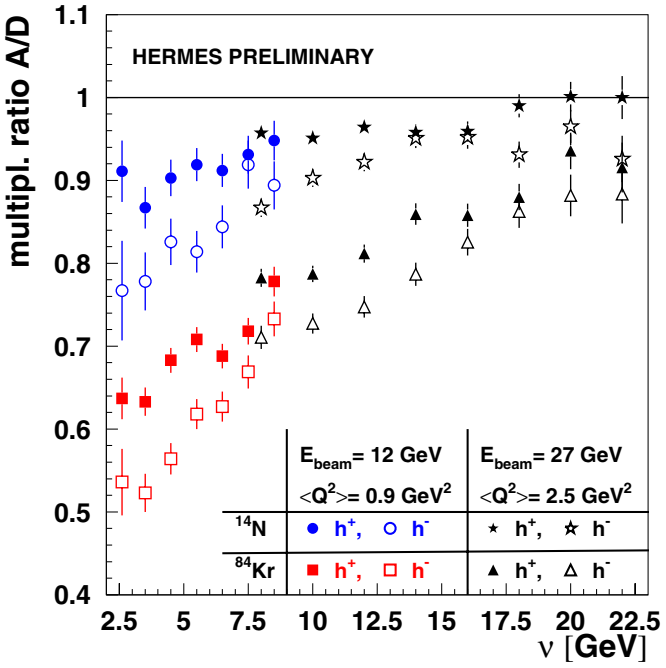

Fig. 5. Hadron attenuation for nitrogen and krypton as a function of ν for the two beam energies 12 GeV and 27.6 GeV

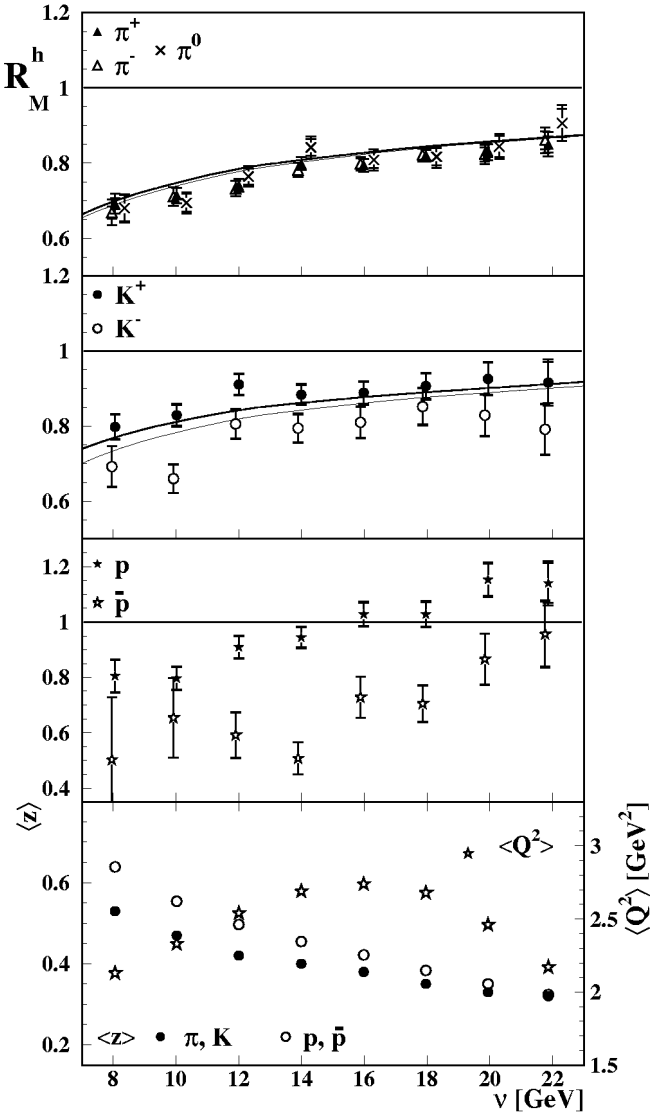

Fig. 6. Hadron attenuation in krypton as a function of ν for a beam energy of 27.6 GeV

possible to accumulate the krypton statistics within a few days. The polarised deuterium data were collected over a period of one year (1999) with an about hundred times less dense polarised target. The yields from deuterium were averaged over the two spin orientations. The 12 GeV data for deuterium, nitrogen and krypton have been obtained in fall 2000, when HERA has operated for a short period at this energy.

In Fig. 5 preliminary results for the multiplicity ratio as a function of ν are shown for both beam energies and for nitrogen and krypton [34].

Following features can be observed: the attenuation effect is substantially stronger for krypton than for nitrogen; for negative hadrons R_M^h decreases continuously with decreasing ν down to values of about 0.5 (0.75) at ν around 0.2 for krypton (nitrogen); at high values of ν the ratio approaches unity, in agreement with earlier EMC data [35], where at ν values around 50 GeV the ratio was compatible with unity for a ^{12}C target and about 0.97 for Cu, indicating that the nuclear effects become very small when the hadron is formed far outside the nucleus and also that effects due to hadron interactions are the dominant source for the attenuation; and there is a significant difference between the ratio for positive and negative hadrons, in agreement with the previously published HERMES data for nitrogen [14].

The ν dependence of the multiplicity ratio for identified pions, kaons, protons and antiprotons for $z > 0.2$ obtained at a beam energy of 27.6 GeV is shown in Fig. 6. The inner (outer) error bars represent the statistical (total) uncertainties, the thick (thin) solid curves represent the calculations of [36] for positive (negative) charge states. In the bottom panel the average z and Q^2 values are displayed for each bin in ν.

The data show the following features: the attenuation ratio increases with increasing ν for all hadron species; R_M^h is identical for positive, negative and neutral pions and also for negative kaons within the total experimental uncertainties, while the attenuation effect for positive kaons is significantly smaller; an even larger difference is observed between protons and antiprotons and between these baryons and mesons. The charge dependence shown in Fig. 5 must therefore be due to positive kaons and protons. These differences can be interpreted in terms of different formation times of baryons and mesons [37], in terms of different hadron-nucleon interaction cross sections or a mixing of quark and gluon fragmentation functions and their modification in nuclei [38].

In Fig. 7 the multiplicity ratios for identified hadrons are presented as a function of z for $\nu > 7GeV$. In the

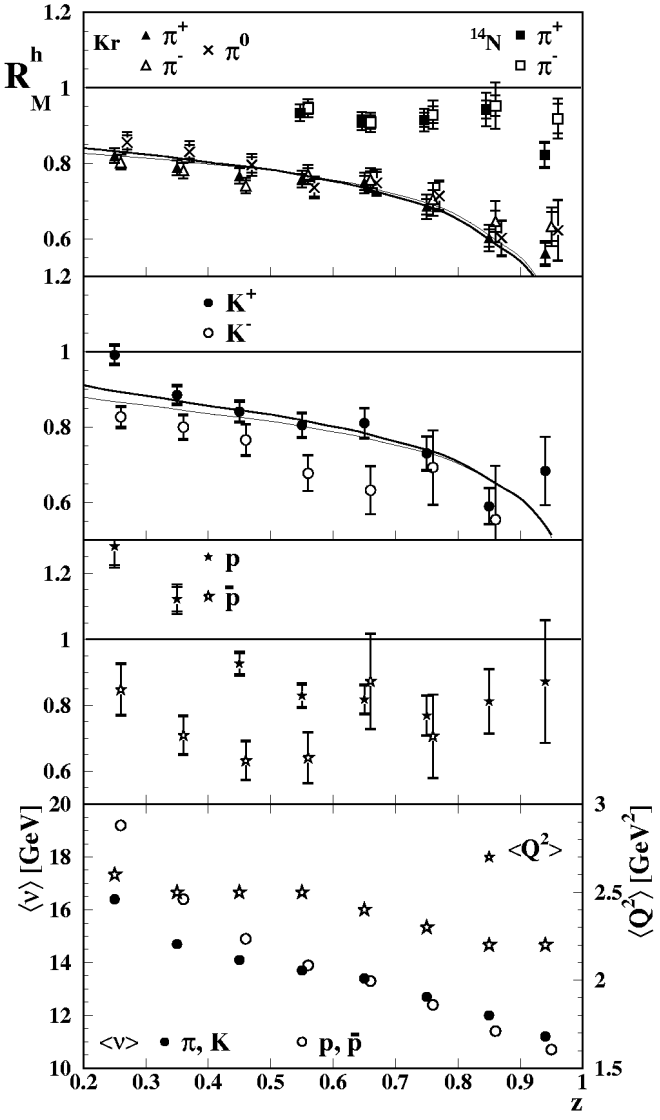

Fig. 7. Hadron attenuation as a function of z for 27.6 GeV

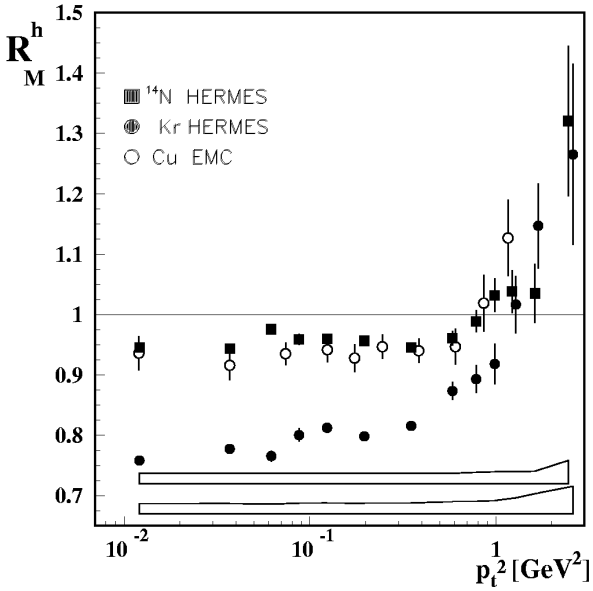

Fig. 8. Hadron attenuation in charged lepton-nucleon scattering as a function of p_t^2

upper panel the ratio for identified charged pions from the reanalysed nitrogen data is also shown for comparison.

At least for the mesons the attenuation ratio decreases substantially with increasing z. An indication of such a behaviour has already been observed in the previously published nitrogen data [14]. It is much stronger and clearly visible in the krypton data. The data are in good agreement with the model calculations of [36], but also in fair agreement with those of the gluon-bremsstrahlung model [39].

The data for identified charged pions for $z > 0.5$ were used to estimate the mass number dependence of the attenuation [40]. They are closer to the $A^{2/3}$-dependence predicted in [38] than to the $A^{1/3}$-dependence expected from models based on nuclear absorption effects only.

In Fig. 8 the multiplicity ratio R_M^h for charged hadrons from ^{14}N and Kr is shown as a function of of the squared transverse hadron momentum, p_t^2, for $\nu > 7$ GeV and $z > 0.2$, together with data from EMC [35] for Cu in the range $10 < \nu < 80$ GeV.

The data for $p_t^2 < 0.7$ GeV^2 show the attenuation discussed above, while at larger values of p_t^2 one observes an enhancement. Such a behaviour can be explained by multiple scattering of the quarks and hadrons propagating in the nuclear medium which broadens the transverse momentum distribution. Such an effect, but larger in magnitude, has been previously observed in hadron-nucleus, and nucleus-nucleus reactions and is known as the Cronin effect [41]. Recent theoretical calculations [42,43] predict this enhancement to occur at a p_t scale of about $1-2$ GeV. These HERMES data may help to interpret the new relativistic heavy-ion results from SPS [44] and RHIC [45], which show a weaker p_t enhancement than expected from the proton-nucleus data.

Acknowledgements. This work was supported by the German Bundesministerium für Bildung und Forschung, BMBF, grant numbers 06 ER 928I and 06 ER 125I.

References

1. K. Ackerstaff et al. (HERMES): Nucl. Instr. and Meth. A **417**, 230-265 (1998)
2. D.P. Barber et al.: Phys. Lett. B **343**, 436-443 (1995)
3. J. Buon and K. Steffen: Nucl. Instr. and Meth. A **245**, 248-261 (1986)
4. C. Baumgarten et al.: Nucl. Instrum. and Meth. A **496**, 277-285 (2003)
5. A. Nass et al.: Nucl. Inst. and Meth. A **505**, 633-644 (2003)
6. C. Baumgarten et al.: Nucl. Instrum. and Meth. A **482**, 606-618 (2002)
7. K. Rith: Prog. Part. Nucl. Phys. **49**, 245-324 (2002)
8. K. Ackerstaff et al. (HERMES): Phys. Rev. Lett. **81**, 5519-5523 (1998)

9. A. Airapetian et al. (HERMES): Eur. Phys. J. C **21**, 599-606 (2001)
10. A. Airapetian et al. (HERMES): Eur. Phys. J. C **17**, 389-398 (2000)
11. A. Airapetian et al. (HERMES): Eur. Phys. J. C **18**, 303-316 (2000)
12. K. Ackerstaff et al. (HERMES): Phys. Rev. Lett. **82**, 3025-3029 (1998)
13. A. Airapetian et al. (HERMES): Phys. Rev. Lett. **90**, 052501, 1-6 (1998)
14. A. Airapetian et al. (HERMES): Eur. Phys. J. C **20**, 479-486 (2001)
15. A. Airapetian et al. (HERMES): hep-ex/0307023
16. W.D. Nowak: these proceedings
17. B. Adeva et al. (SMC): Phys. Rev. D **58**, 112001, 1-17 (1998)
18. K. Abe et al. (SLAC-E143): Phys. Rev. D **58**, 112003, 1-54 (1998)
19. P.L. Anthony et al. (SLAC-E155): Phys. Lett. B **463**, 339-345 (1999)
20. A. Airapetian et al. (HERMES): Phys. Lett. B **442**, 484-492 (1998)
21. B. Adeva et al. (SMC): Phys. Rev. D **60**, 072004, 1-9 (1999); Phys. Rev. D **62**, 079902, 1-2(E) (2000)
22. P.L. Anthony et al. (SLAC-E155): Phys. Lett. B **493**, 19-29 (2000)
23. B. Adeva et al. (SMC): Phys. Rev. D **58**, 112002, 1-15 (1998)
24. Y. Goto et al.: Phys. Rev. D **62**, 034017, 1-18 (2000)
25. M. Glück et al.: Phys. Rev. D **63**, 094005, 1-12 (2001)
26. J. Blümlein and H. Böttcher: Nucl. Phys. B **636**, 225-263 (2002)
27. K. Ackerstaff et al. (HERMES): Phys. Lett. B **464**, 123-134 (1999)
28. A. Airapetian et al. (HERMES): hep-ex/0307064
29. H.L. Lai et al.: Eur. Phys. J. C **12**, 375-392 (2000)
30. B. Dressler et al.: Eur. Phys. J. C **14**, 147-157 (2000)
31. R. Baier, D. Schiff, and B.G. Zakharov: Ann. Rev. of Nucl. and Part. Science **50**, 37-69 (2000)
32. B.Z. Kopeliovich: these proceedings
33. N. Akopov et al.: Nucl. Instr. and Meth. A **479**, 511-530 (2002)
34. P. van der Nat: Master's thesis, University of Amsterdam, July 2002
35. J. Ashman et al. (EMC): Z. Phys. C **52**, 1-11 (1991)
36. A. Accardi, V. Muccifora, and H.J. Pirner: Nucl. Phys. A **720**, 131-156 (2003)
37. B.Z. Kopeliovich and F. Niedermayer: Phys. Lett. B **151**, 437-438 (1985)
38. X.N. Wang and X. Guo: Nucl. Phys. A **696**, 788-832 (2001); E. Wang and X.N. Wang: Phys. Rev. Lett. **89**, 162301, 1-4 (2002)
39. B.Z. Kopeliovich, J. Nemchik, and E. Predazzi: *Proceedings of the workshop on Future Physics at HERA, Vol. 2*, G. Ingelman, A. De Roeck, and R. Klanner, eds. (DESY 1995/1996) 1038-1042 and nucl-th/9607036
40. E. Garutti: Ph.D thesis, University of Amsterdam, March 2003
41. J.W. Cronin et al.: Phys. Rev. D **11**, 3105-3123 (1975)
42. E. Wang and X.N. Wang: Phys. Rev. C **64**, 034901, 1-8 (2001)
43. B.Z. Kopeliovich et al.: Phys. Rev. Lett. **88**, 232303, 1-4 (2002)
44. M.M. Aggarwal et al. (WA98): Phys. Rev. Lett. **81**, 4087-4091 (1998); and **84**, 578-579(E) (2000); H. Appelshauser et al. (NA49): Phys. Rev. Lett. **82**, 2471-2475 (1999); G. Agakishiev et al. (CERES): hep-ex/0003012
45. K. Adcox et al. (PHENIX): Phys. Rev. Lett. **88**, 022301, 1-6 (2002)